A Dynamical Feedback Model for Adaptation in the Olfactory Transduction Pathway

Giovanna De Palo,[†] Anna Boccaccio,[†‡] Andrew Miri,[†] Anna Menini,[†§] and Claudio Altafini[†*]
[†]International School for Advanced Studies, Trieste, Italy; [‡]Istituto di Biofisica, National Research Council, Genoa, Italy; and [§]Italian Institute of Technology, Genoa, Italy

ABSTRACT Olfactory transduction exhibits two distinct types of adaptation, which we denote multipulse and step adaptation. In terms of measured transduction current, multipulse adaptation appears as a decrease in the amplitude of the second of two consecutive responses when the olfactory neuron is stimulated with two brief pulses. Step adaptation occurs in response to a sustained steplike stimulation and is characterized by a return to a steady-state current amplitude close to the prestimulus value, after a transient peak. In this article, we formulate a dynamical model of the olfactory transduction pathway, which includes the kinetics of the CNG channels, the concentration of Ca ions flowing through them, and the Ca-complexes responsible for the regulation. Based on this model, a common dynamical explanation for the two types of adaptation is suggested. We show that both forms of adaptation can be well described using different time constants for the kinetics of Ca ions (faster) and the kinetics of the feedback mechanisms (slower). The model is validated on experimental data collected in voltage-clamp conditions using different techniques and animal species.

INTRODUCTION

To optimize the signal/noise-ratio over a range of input intensities, vertebrate sensory neurons (olfactory, visual, and auditory; see Torre et al. (1)) are able to adjust their dynamical range maintaining the response around a nominal value, while their input stimulus changes considerably. Sliding the window of interest maximizes the capacity for distinguishing variations of a signal while avoiding distortions due to saturation. In the biological literature, this process is called adaptation (1–3). Many biological systems are known to adapt, and significant examples include various signal transduction pathways (1,2) and bacterial chemotaxis (4,5).

In olfactory transduction, the ordinary input to an olfactory sensory neuron (OSN, here, the sensor) consists of a stimulation by odorant molecules eventually leading to an electrical signal. Here we consider the transduction current measured with the voltage clamped at a constant value as the measurable output of the pathway (see the Supporting Material for details). Two forms of adaptation of the odorant-induced current response (6–9) are observed during two types of experimental protocols:

1. Step adaptation, which is caused by a sustained stimulus (a step input) and consists of a decline in the response despite the continued presence of a constant odorant stimulus;
2. Multipulse adaptation, which is caused by repeated brief stimuli and involves a reduction in the amplitude of the response to the second odorant stimulus with respect to the first. The difference in amplitude of the responses is reduced when the time interval between stimuli is increased; complete recovery of the response is seen for a sufficiently long interval.

In step adaptation, the return of the transduction current toward the basal prestimulus level implies that the system has a memory of the basal level and a mechanism enabling regulation around it. Multipulse adaptation in OSNs also represents a form of memory: the attenuation of the transduction current in response to the second pulse means that, in this case, the past history of the system can also influence its present behavior (6). Despite the evidently similar nature of the two phenomena, mathematical models taking into account both forms of adaptation are very rare (the only articles we know of are Dougherty et al. (10) and Reidl et al. (11)). The aim of this article is to provide insight into the mechanism of step and multipulse adaptation by constructing a mathematical model of the olfactory transduction pathway that reproduces these phenomena.

Several mathematical models capturing step adaptation have been reported in the literature (2,4,5,12–14). Most of these models describe kinetic mechanisms suitable to attain perfect adaptation, in which a new steady-state value exactly corresponds to the prestimulus value. In voltage-clamp experiments on OSNs, however, step adaptation is never perfect: a (small) difference between the prestimulus value of the current and the new steady-state value achieved after a steplike stimulation is always observed (6,15), with an amplitude that typically grows with the size of the step (see Menini et al. (15), Fig. 1). We will show here that imperfect step adaptation and multipulse adaptation can be explained by the same mechanism.

Submitted November 10, 2011, and accepted for publication April 25, 2012.

*Correspondence: altafini@sissa.it

Andrew Miri's present address is Howard Hughes Medical Institute, Departments of Neuroscience and Biochemistry and Molecular Biophysics, Columbia University, New York, NY.

Editor: Michael Stern.

0006-3495/12/06/2677/10 $2.00

doi: 10.1016/j.bpj.2012.04.040

Conceptually, our model derives from the integral feedback model of Yi et al. (5). In this scheme, feedback evokes temporal integration of the past history of the output to force it to return to its prestimulus value. For systems in which the signals have constant sign (positive concentrations), a perfect memory of the past implies a feedback variable that is monotonically increasing. However, in olfactory transduction, the strength of adaptation in a multipulse protocol decays as the interpulse interval increases, meaning that the memory of the past is gradually forgotten by the system. An exact integral feedback adaptation cannot capture this feature, just like it does not predict the displacement between steady state and prestimulus value in the step adaptation. However, if we add a memory decay to the integral feedback model, its monotonic character is lost and both types of adaptation can be correctly reproduced.

Olfactory transduction occurs in the cilia of OSNs. The cilia contain all the biochemical machinery for transduction and two types of ion channels: cyclic nucleotide-gated (CNG) and Ca-gated Cl channels (see Fig. 1). Voltage-gated channels for the generation of action potentials are located in other compartments of OSNs and are not activated when the voltage is clamped at a constant value, thereby decoupling the olfactory transduction process from the spiking events. The main steps of olfactory transduction involve the binding of extracellular odorant molecules to odorant receptors, which induces intracellularly a G-protein-mediated activation of adenylyl cyclase (AC) to produce cyclic AMP (cAMP). cAMP then directly gates CNG channels, causing an influx of Na and Ca ions. Ca entry amplifies the response by gating a Cl current and, in combination with Ca-binding proteins, induces feedback mechanisms: Ca-calmodulin (CaCaM) increases the phosphodiesterase (PDE) hydrolysis of cAMP, and activates CaCaM-dependent protein kinase II (CaMKII), which inhibits AC. Moreover, the cAMP sensitivity of the CNG channels is reduced by Ca feedback mediated by CaCaM and/or other Ca-binding proteins natively bound to the CNG channels (for reviews, see Schild and Restrepo (16) and Kleene (17)).

Previous experiments have shown that the shape of the response to odorants can be reproduced by increasing the concentration of cAMP in the cilia via photorelease of caged cAMP (see Fig. 4 of Takeuchi and Kurahashi (18), or Fig. 2 of Kurahashi and Menini (7)), indicating that the response time course is not significantly altered by the events occurring in the pathway upstream of the production of cAMP (receptor activation, G-protein, and AC signaling). Furthermore, it has been shown that the principal molecular mechanisms underlying multipulse odorant adaptation occur after the production of cAMP, because the responses to repeated photorelease of cAMP have adaptation properties similar to those induced by odorants (7). We therefore decided to

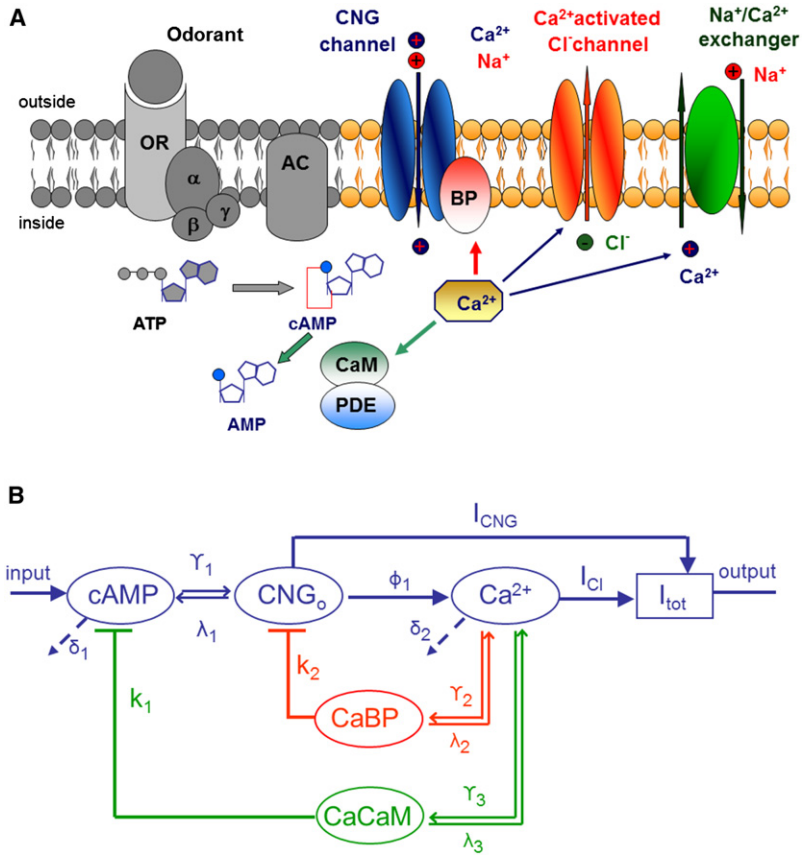

FIGURE 1 The pathway and its feedback loops. (*A*) Representation of the entire olfactory transduction pathway in the cilia of OSNs. Modified from Pifferi et al. (38), with permission. The shaded part is not considered in this study. A detailed description of the pathway is provided in the Supporting Material. (*B*) Scheme of the basic reactions and feedback mechanisms included in our model. Pointed arrows mean positive regulation, stopped arrows mean negative feedbacks, dashed arrows degradations. The three bidirectional arrows represent reversible reactions. The two feedback loops are represented in red and green.

focus our study on the part of the pathway downstream of the production of cAMP, where Ca-mediated regulatory mechanisms play a key role. Ca-induced feedbacks are crucial for adaptation: indeed, it has been shown that in the absence of Ca influx, achieved either by removing Ca from the extracellular solution (6,19) or by recording the current at positive membrane potentials (20), neither form of adaptation can take place.

The common dynamical explanation for both types of adaptation provided in this article relies on the kinetics of the Ca-induced feedback being slower than the kinetics of the gating of the CNG channels and Ca influx through CNG channels. We will show that by modulating the time constants of these kinetics with respect to the other time constants of the system, a trade-off between the two forms of adaptation is established. For example, assuming a very long time constant for the feedback results in a nearly exact step adaptation, but in an amplitude recovery of multipulse adaptation that is slower than that observed experimentally. On the contrary, assuming a short time constant for the feedback leads to incomplete step adaptation but to faster recovery in multipulse adaptation. This trade-off implicitly constrains the range of values of the parameters in which the behavior of the model reflects the experimental data. We show here that for both input protocols (sustained and repeated stimuli), a variety of data obtained in different experimental conditions (different species; stimulation by odorant or by direct release of second messengers) lead to fairly similar values of the parameters. Our results demonstrate that both types of adaptation can be reproduced correctly if the system is endowed with multiple timescales, such that the regulatory actions have longer time constants than the direct transduction of stimuli to membrane current. This kinetic property is the basis for several models proposed for (step) adaptation (13,14), and is also consistent with hypotheses presented in the olfactory transduction literature ((21), see also Reidl et al. (11)).

MATERIALS AND METHODS

Patch-clamp experiments were performed on OSNs dissociated from the olfactory epithelium of newts (*Cynops pyrrhogaster*, as described in Kurahashi and Menini (7) and Kurahashi (22)), salamanders (*Ambystoma tigrinum*, as described in Menini et al. (15) and Firestein et al. (23)), or mice (BALB/c strain, as described in Lagostena and Menini (8)). Transduction currents were elicited by 1), odorant, 2), photorelease of cAMP (7,20) or of its nonhydrolyzable form 8-Br-cAMP (20), and 3), 3-isobutil-1- methylxanthine (IBMX, a membrane-permeable PDE inhibitor). Currents were recorded in the whole-cell voltage-clamp configuration at a holding potential of −50 mV. For details, see the Supporting Material.

RESULTS

Description of the model

Fig. 1 *A* illustrates the main steps of the olfactory transduction cascade (see also the Supporting Material for a detailed description). We focused our study on the part of the pathway downstream of the production of cAMP and considered experimental data obtained using a constant voltage protocol (thus the voltage dependence does not appear in the model proposed here). Hence, here the open-loop part of the pathway (the signaling cascade from the input stimulus to the output current, feedback excluded) consists of the cAMP-induced opening of the CNG channels and the influx of Ca into the cilia, whereas the feedback part involves the Ca-binding proteins, which directly (through their gating action on the CNG channels) or indirectly (through the activation of PDE) leads to the closure of the CNG channels. Both feedback actions are subordinated to Ca influx.

The model of ordinary differential equations we use consists of the following five state variables:

1. cAMP, the concentration of the cyclic nucleotide,
2. CNG_o, the concentration of open CNG channels,
3. Ca, the concentration of Ca free ions,
4. CaBP, the concentration of the complex formed by Ca and Ca-binding protein (BP) natively bound to CNG channels, and
5. CaCaM, the concentration of the cytoplasmic Ca-calmodulin complex.

CaCaM is taken here as a proxy for the PDE activity (not modeled explicitly), and the complex CaCaM is assumed to be free in the ciliary cytoplasm. It is known that Ca-free calmodulin is also preassociated with CNG channels and facilitates a rapid Ca-dependent reduction in cAMP sensitivity of the CNG channels (24). However, because calmodulin may not be the only protein involved in this process (25), we take a more general perspective and attribute the reduction in sensitivity for cAMP of the CNG channels to a generic BP natively bound to the channels and whose action is triggered by Ca. Thus the variable CaBP summarizes the effect of potentially more than one type of Ca-binding proteins (including also calmodulin) that are assumed to be permanently bound to the CNG channels and able to rapidly reduce their sensitivity for cyclic nucleotides when activated by the binding with Ca. Whereas the first three variables form the open-loop part of the model, the pair CaCaM and CaBP indicates our feedback variables (Fig. 1 *B*). Their action in generating dynamical feedback can be formulated using ordinary differential equations:

$$\frac{d\mathrm{cAMP}}{dt} = 2\lambda_1 \cdot \mathrm{CNG_o} - 2\gamma_1 \cdot \mathrm{cAMP}^2(\mathrm{CNG_{tot}} - \mathrm{CNG_o}) - \delta_1 \cdot \mathrm{cAMP} - f_1(\mathrm{cAMP}, \mathrm{CaCaM}) + u, \quad (1)$$

$$\frac{d\mathrm{CNG_o}}{dt} = \gamma_1 \cdot \mathrm{cAMP}^2(\mathrm{CNG_{tot}} - \mathrm{CNG_o}) - \lambda_1 \cdot \mathrm{CNG_o} - f_2(\mathrm{CNG_o}, \mathrm{CaBP}), \quad (2)$$

$$\frac{d\mathrm{Ca}}{dt} = \phi_1 \cdot \mathrm{CNG_o} - \delta_2 \cdot \mathrm{Ca} - \gamma_2 \cdot \mathrm{Ca}(\mathrm{BP_{tot}} - \mathrm{CaBP}) + \lambda_2 \cdot \mathrm{CaBP} - 2\gamma_3 \cdot \mathrm{Ca}^2(\mathrm{CaM_{tot}} - \mathrm{CaCaM}) + 2\lambda_3 \cdot \mathrm{CaCaM}, \quad (3)$$

$$\frac{d\mathrm{CaBP}}{dt} = \gamma_2 \cdot \mathrm{Ca}(\mathrm{BP_{tot}} - \mathrm{CaBP}) - \lambda_2 \cdot \mathrm{CaBP}, \quad (4)$$

$$\frac{d\mathrm{CaCaM}}{dt} = \gamma_3 \cdot \mathrm{Ca}^2(\mathrm{CaM_{tot}} - \mathrm{CaCaM}) - \lambda_3 \cdot \mathrm{CaCaM}. \quad (5)$$

Here, the initial concentrations correspond to a basal prestimulus level.

In Eqs. 1–5, the total concentrations of the CNG channels ($\mathrm{CNG_{tot}}$), calmodulin ($\mathrm{CaM_{tot}}$), and the Ca-binding proteins ($\mathrm{BP_{tot}}$) are conserved. No conservation law is imposed on the low-molecular-weight cAMP and Ca. Mass-action kinetics is assumed for binding reactions (see Supporting Material). The input stimulus u appears as a synthesis term in Eq. 1 for cAMP, having distinct temporal profiles for the different stimuli used (see the Supporting Material). Two more terms in Eq. 1 describe the binding/unbinding of cAMP to the CNG channels (the term $\mathrm{CNG_{tot}}$-$\mathrm{CNG_o}$ represents the concentration of closed channels). Equation 1 also involves a linear degradation term representing the diffusion of the nucleotide away from the internal membrane surface, and a negative feedback term due to the hydrolysis induced (through PDE) by the CaCaM complex (*green stopped arrow* in Fig. 1 *B*). The simplest way to represent this feedback action avoids modeling explicitly PDE and is given by

$$f_1(\mathrm{cAMP}, \mathrm{CaCaM}) = k_1 \cdot \mathrm{cAMP} \cdot \mathrm{CaCaM}. \quad (6)$$

To describe the opening rate of the CNG channels in Eq. 2, we use a mass-action law with cooperativity index 2 for cAMP because the binding of two molecules of cAMP is sufficient to open the channel (17,26,27). In Eq. 2, besides the association/dissociation with cAMP, $\mathrm{CNG_o}$ decreases due to negative feedback of the CaBP complex (*red feedback loop* in Fig. 1 *B*).This negative gating activates only when Ca binds to the Ca-binding proteins permanently attached to the CNG channel. The simplest possible functional form to express this feedback is

$$f_2(\mathrm{CNG_o}, \mathrm{CaBP}) = k_2 \cdot \mathrm{CNG_o} \cdot \mathrm{CaBP}^2, \quad (7)$$

where a cooperativity index 2 is assumed for CaBP to account for the possible presence of multiple units of BP in the complex they form with the CNG channels, as reported for example for calmodulin (24,28). An alternative model to describe this negative gating is mentioned later on and discussed more in detail in the Supporting Material.

Equation 3 represents the inflow of free Ca ions into the cilia that depends on $\mathrm{CNG_o}$, on their diffusion away from the internal membrane surface (and extrusion through the Na/Ca exchanger), and on their binding/unbinding with calmodulin and Ca-binding proteins. The remaining Eqs. 4 and 5 for CaBP and CaCaM represent mass action laws for the binding and unbinding of Ca ions. For simplicity we assume a linear behavior between Ca and BP, while for the binding to CaM, following Reidl et al. (11), we consider a cooperativity index equal to 2 (the four binding sites for Ca are highly cooperative in pairs, see Park et al. (29)).

The total elicited transduction current (the output measured in experiments) is the sum of two distinct inward currents: one component carried by the influx of Na and Ca through CNG channels and the other carried by the efflux of Cl through channels gated by Ca. The equations for the currents are therefore

$$I_{\mathrm{CNG}} = k_c \cdot I_{\max} \cdot \mathrm{CNG_o}, \quad (8)$$

$$I_{\mathrm{Cl}} = (1 - k_c) \cdot I_{\max} \left(\frac{\mathrm{Ca}^2}{\mathrm{Ca}^2 + k_{1/2}^2} \right). \quad (9)$$

Thus, the output of our model is given by the sum of I_{CNG} and I_{Cl}. The constant k_c, representing the relative contribution of the two currents, is known to be ~20% in the case of a nearly saturating response (30). I_{CNG} depends on the number of open channels and we use a direct proportionality with $\mathrm{CNG_o}$. I_{Cl} depends on the fraction of open Cl channels, which is a function of the Ca concentration (31) described by a Hill-equation with a cooperativity index of 2 (17,20).

Further details about the model are provided in the Supporting Material.

Description of the experiments

To test the ability of the model to reproduce the adaptation of OSN responses, we considered data from various experimental conditions in which responses were elicited by different stimuli: 1) odorant; 2) photorelease of caged cyclic nucleotides, either cAMP or 8-Br-cAMP; and 3) IBMX. Experimental data obtained with odorant stimulation and with photorelease of cAMP or 8-Br-cAMP (Figs. 2 and 3) are reproduced from our previously published studies (7,15,20), while data using IBMX (Fig. 4) are our original results. All experiments considered here were performed in voltage-clamp conditions, holding the membrane voltage constant at −50 mV for the entire duration of the experiment. This allows the measurement of transduction currents without the interference of action potentials.

1. Response to odorant. A typical example of multipulse odorant adaptation in an OSN is illustrated in Fig. 2 *A*. Responses to pairs of identical odorant pulses separated by a variable time interval Δt are plotted superimposed.

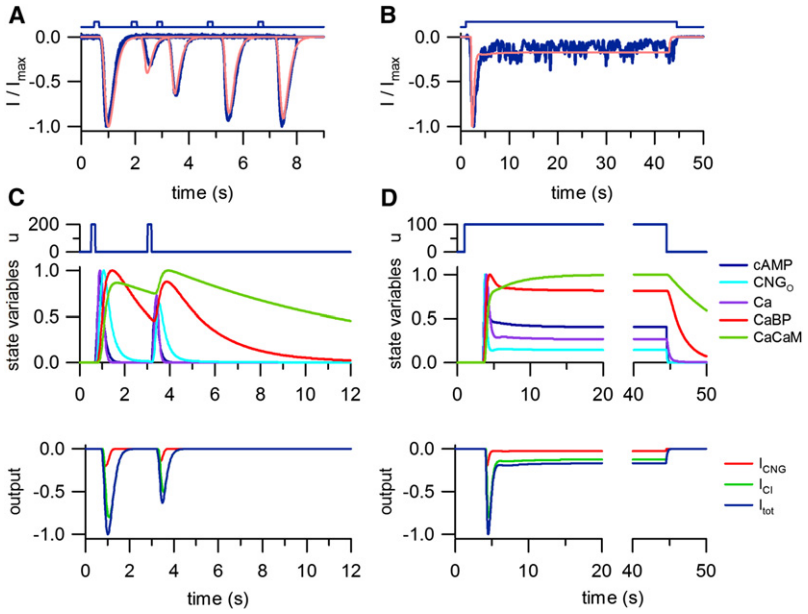

FIGURE 2 Response to odorant. (*A*) Response reductions by a conditioning pulse and their recovery time course in newt OSN (*blue*) and the corresponding fit of the model (*red*). (The *blue traces* above the fit of the data represent the timing of the odorant stimulations.) The amplitude of each response was normalized to the response to the first conditioning pulse. Two identical odorant stimuli of amyl acetate of 200-ms duration were applied separated by a time interval Δt of 2.5, 4.5, and 6.5 s. Experimental data drawn from Kurahashi and Menini (7) with permission from Macmillan Publishers. (*B*) The response of a salamander OSN to an odorant stimulus sustained for 43.5 s. Experimental data adapted from Menini et al. (15) with permission from Macmillan Publishers. (*C*) Corresponding simulated input, normalized state variables, and output currents (with the two components I_{CNG} and I_{Cl}) for the pulse pair with Δt = 2.5 s shown in panel *A*. (*D*) Simulated input, normalized state variables, and output currents (I_{CNG} and I_{Cl}) for a sustained stimulus of 43.5 s in duration.

The amplitude of the response to the second pulse is reduced with respect to the first, and progressively recovers to the initial value as Δt is increased. The input is modeled as a pair of square pulses of the same duration and Δt as the experimentally delivered odorant pulses (see the Supporting Material for a discussion of the choice of the input pulse). Fig. 2 *B* shows an example of step odorant adaptation. The current response declines to an almost basal steady-state level despite the persistent odorant stimulus.

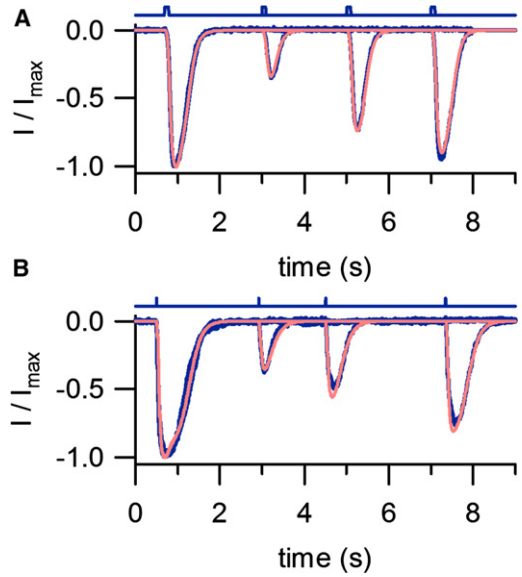

FIGURE 3 Response to photorelease of caged cyclic nucleotides. Response reductions by a conditioning pulse and their recovery time course in OSNs. (*Color online*: the experimental data are shown in *blue*, the response of the model in *red*.) Above each panel, the experimental input is shown (see Fig. S3 for the simulated input). In each panel, the amplitudes of the responses were normalized to the response to the first conditioning pulse. (*A*) Responses of a newt OSN to photorelease of cAMP by two identical 100-ms ultraviolet flashes, separated by increasing time intervals Δt of 2.3, 4.3, and 6.3 s. Experimental data adapted from Kurahashi and Menini (7) with permission from Macmillan Publishers. (*B*) Responses of a mouse OSN to photorelease of 8-Br-cAMP obtained with two identical ultraviolet-light flashes of 1.5 ms separated by time intervals of 2.5, 4, and 6.8 s. Experimental data from Boccaccio et al. (20), reproduced with permission.

2. Response to photorelease of caged compounds. The stimulus is given by the photorelease of caged cyclic-nucleotides: in Fig. 3 *A*, cAMP is released with 100-ms light flashes, whereas in Fig. 3 *B* the nonhydrolyzable 8-Br-cAMP is released with briefer, ~1.5 ms, but more intense flashes. The input is modeled as a pair of square pulses of a similar duration and the same Δt as in the experiments. For both types of caged compounds, we assume that the concentration of the cyclic nucleotide depends on the intensity and duration of the different flashes. As 8-Br-cAMP is not hydrolyzable by PDE (32,33), we consider PDE to be inactive in this case, and therefore the CaCaM feedback is absent from the model. Multipulse adaptation similar to that observed with odorants is seen with photorelease of both cAMP and of 8-Br-cAMP.
3. Response to IBMX. Fig. 4 shows responses to applications of IBMX. Because IBMX reduces the activity of PDE, responses in the presence of IBMX are caused by the increase in cAMP concentration produced by the basal activity of AC. Stimulus onset is modeled with a rapid rise in u; its offset is modeled as a slow decay (see Fig. S1, Fig. S4, and Table S1 in the Supporting Material for an explanation). Fig. 4 *A* shows superimposed current recordings in response to pairs of brief stimuli with increasing Δt. Fig. 4 *B* shows the response of a neuron to a prolonged IBMX stimulation. The current response recovers to a low steady-state level

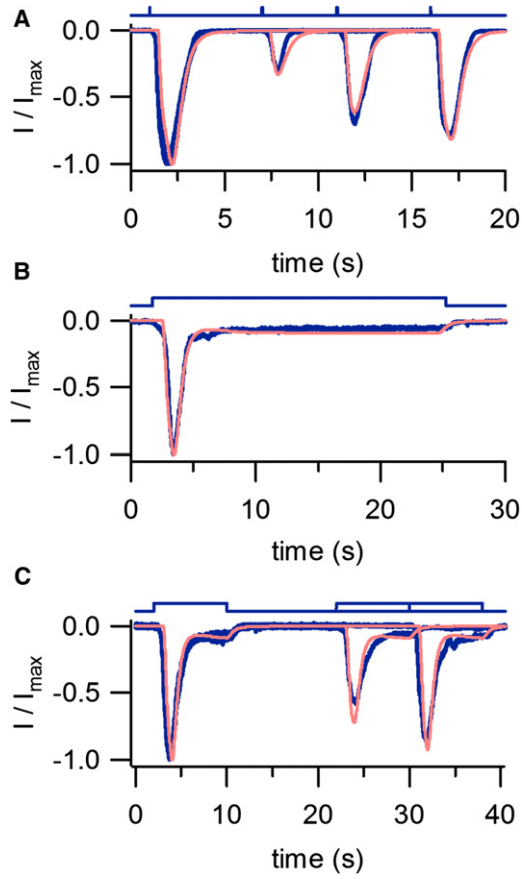

FIGURE 4 Response to IBMX. Responses of salamander OSNs to IBMX. (*On-line color version: blue*) Experimental data; (*red*) response of the model. Above each panel, the experimental input is shown (see Fig. S4 for the simulated input). (*A*) Responses to repeated applications of IBMX pulses of 20 ms applied to the cell at time intervals Δt of 6, 10, and 15 s. (*B*) Response to an IBMX stimulus applied for 24 s. (*C*) Responses to two subsequent prolonged IBMX stimuli of 8 s duration with interpulse interval of 20 and 28 s. IBMX was applied through a glass pipette controlled by a pressure ejection system. The concentration of IBMX in the pipette was 0.1 mM. Both kinds of adaptation are observed in the experiments and reproduced by the model: decline of the peak and convergence to a new adapted steady state within each stimulation, and peak amplitude modulation depending on the interstimuli lag time.

although the stimulus is maintained. Fig. 4 *C* shows the superimposed responses to two identical prolonged IBMX applications separated by Δt of 20 or 28 s. The current response to the first stimulus transiently increases and then decays to a steady state during the sustained stimulus. The amplitude of the transient response to a second stimulus increases as Δt increases, as for the experiments shown in Fig. 2 *A*, Fig. 3, and Fig. 4 *A*.

Parameter fitting

The model of Eqs. 1–9 contains 18 parameters (plus five describing the input profiles, see Table S1). These parameters are reported in Table 1. A priori knowledge on some of these parameters is available or can be inferred from other experiments. The parameters δ_1, λ_1, and γ_1 were previously estimated from experiments in low calcium conditions (see Fig. S2 in the Supporting Material). The value k_c is drawn from Boccaccio and Menini (30) and Gu et al. (34), and I_{max} is set equal to 1 because we considered normalized currents. The parameter $k_{1/2}$ is constrained to be between 2 and 5 (17,20), and the total concentration of calcium-binding proteins BP_{tot} bound to CNG channels is constrained by its stoichiometric ratio with CNG_{tot}. The relative blockage B of the CaCaM feedback due to the action of IBMX was allowed to vary between 0.6 and 1.

Numerical values of the remaining parameters were obtained by fitting Eqs. 1–9 to the various types of experimental time series described above using a nonlinear least-squares algorithm (see the Supporting Material for details). For each of the four different types of input (odorant, caged cAMP, caged 8-Br-cAMP, and IBMX), we estimated a distinct set of parameters. Apart from the different effect (and entry point) of the four types of inputs, this choice originates also from the different animal cells used in the various sets of experiments.

The four parameter sets, reported in Table 1, show a substantial agreement. They are also in agreement with the parameter values one obtains performing a fit on all data simultaneously (see Common column in Table 1). Because the model is nonlinear, no globally convergent fitting procedure exists. However, an extensive search over the space of parameters (see Fig. S8 and Fig. S9) suggests that the parameter region that optimizes the least-squares cost functional may be uniquely defined for most of the parameters. A notable exception is λ_3, the dissociation rate for the CaCaM feedback, whose value appears not to be univocally determined by the optimization procedure. No ambiguity is present in the 8-Br-cAMP responses, because in this case the CaCaM feedback is absent. We comment on this in the Discussion section.

Further details about the fitting procedure are given in the Supporting Material.

Validation of the model

The agreement between parameter estimates across input types is quite good, despite the fact that different experimental techniques and animal species were used and despite the absence of step adaptation for two of the input types. This demonstrates that similar dynamics can account for all of the experimental time series we fit. In particular, the four parameter sets unanimously agree on the following relationship among degradation and dissociation rates: $0 < \lambda_2, \lambda_3 \ll \delta_2$. This corresponds to saying that the time constants of the feedback variables CaBP and CaCaM are much longer than that of free Ca.

Fig. 2, *C* and *D*, shows the temporal profile for the state variables from fits to data shown in Fig. 2, *A* and *B*. The

TABLE 1 Parameter sets used to fit the data

Name	Function	Odor	cAMP	8-Br-cAMP	IBMX	Common (SD)	Details
δ_1	Degradation rate of cAMP/8-Br-cAMP	3.16	2.91	3.06	4.00	4.56 (0.03)	Low Ca exps
k_1	CaCaM feedback gain	47.02	29.57		49.98	12.58 (9.46)	
λ_1	Dissociation rate between CNG and cAMP	0.63	0.33	0.33	0.22	1.82 (0.01)	Low Ca exps
γ_1	Association rate between CNG and cAMP	0.08	0.04	0.09	0.09	0.06 (0.0003)	Low Ca exps
k_2	CaBP feedback gain	163.17	87.01	84.17	134.22	181.39 (19.56)	
ϕ_1	Inflow of Ca through CNG channels	47.29	55.85	36.80	15.46	13.50 (0.41)	
δ_2	Outflow of Ca	3.32	5.07	3.48	1.35	2.98 (0.03)	
γ_2	Association rate of Ca and BP	0.84	0.30	0.14	0.10	0.16 (0.005)	
λ_2	Dissociation rate of CaBP	0.60	0.42	0.16	0.25	0.12 (0.001)	≥ 0.1
γ_3	Association rate of Ca and CaM	0.01	0.21		1.00	0.01 (0.05)	
λ_3	Dissociation rate of CaCaM	0.10	0.33		0.20	0.10 (0.03)	≥ 0.1
k_c	Percentage of I_{CNG} in the total current	0.2					(30,34)
I_{max}	Maximum amplitude of the total current	1					Normalized
$k_{1/2}$	Half-maximum activation of I_{Cl} due to Ca	4.03	2.91	3.60	4.34	4.92 (0.13)	(17,20)
B	Relative blockage due to IBMX				0.75	0.60 (0.09)	≥ 0.6
CNG_{tot}	Total concentration of CNG channels	0.74	1.22	5.72	1.00	1.10 (0.01)	
BP_{tot}	Total concentration of Ca binding protein	0.74	1.19	1.33	1.00	1.10 (0.01)	$\leq 2CNG_{tot}$
CaM_{tot}	Total concentration of calcium calmodulin	1.30	0.84	1.00	1.50	0.68 (2.82)	

Parameter names, meaning, and values are reported. The values for the four input types are reported in the first four columns (see Figs. 2–4), while the fifth column contains the common parameter set, used to fit all the data simultaneously (see Fig. S5, Fig. S6, and Fig. S7, and the corresponding explanations). For the Common column, the standard deviation (SD) is reported. The parameters with the largest error (k_1, λ_3, and CaM_{tot}) are all involved in the feedback loop of CaCaM. These uncertainties in the parameter estimation can be deduced also from the flat profiles of the cost function around the optimal values of the parameters in Fig. S8. It is a consequence of the redundancy of the two feedback loops. Errors are similar for the other parameter sets. In the last column, we collect all a priori information available on the parameters, as well as all constraints imposed in our fitting procedure. The term "Low Ca exps" refers to parameters estimated in low-calcium experiments (see the Supporting Material).

response of the open-loop part of the pathway, involving cAMP, CNG_o, and Ca, is prompter than that of the feedback variables CaBP and CaCaM, both in growth and decay. For multipulse adaptation, in particular, if the concentrations of CaBP and CaCaM are still above their basal levels when the second pulse arrives, the transient excursion of the pulse response of the open loop part is reduced because the feedback response is quicker. The result is that for both CNG_o and Ca the second pulse is attenuated with respect to the first. In the case of step adaptation in Fig. 2 *B*, the early response consists of a transient peak of cAMP, CNG_o, and Ca. As the concentration of the two feedback variables CaBP and CaCaM builds up, the corresponding negative feedbacks start influencing the dynamics of the open loop cascade, progressively curtailing the transient excursion, until a steady state is reached. At this steady state, the concentration of the feedback variables is still high, whereas both CNG_o and Ca have returned near their basal levels. In turn, from Eqs. 8 and 9 this implies that the output current returns near its basal level. Similarly, when the input step finishes, the open-loop variables drop to their basal levels much quicker than the feedback quantities.

For photorelease of 8-Br-cAMP, even if PDE activity is absent (no CaCaM feedback in the model, $k_1 = 0$), CaBP feedback is enough to guarantee multipulse adaptation (Fig. 3 *B*). However, a comparison between the models for cAMP and for 8-Br-cAMP photorelease data (Fig. 3, *A* and *B*) indicates that the joint action of both feedback mechanisms yields a more rapid recovery of the response. In the model, when the contribution of CaCaM is suppressed, the decaying phase of the cyclic nucleotide concentration becomes slower, modifying the kinetics of all the processes downstream (see Fig. S3).

Fig. 4 *C* illustrates a situation in which both types of adaptation are observed in response to IBMX stimulation. Given the dissociation rate constants for CaBP and CaCaM inferred from data, the recovery from multipulse adaptation is almost complete when Δt is 15 s or longer (Figs. 2 *A* and 4 *A*). In Fig. 4 *C*, however, Δt for the first pair of steps is 20 s but adaptation is still clearly visible, much more than when $\Delta t = 28$ s. This apparent discrepancy is interpretable in terms of the model of Eqs. 1–7. During a step response, the feedback variables CaBP and CaCaM remain at high concentrations, and only after stimulus offset do they start to decrease (see Fig. S4). Hence essentially only the lag time between the end of the first step and the beginning of the second matters in determining the magnitude of multipulse adaptation.

Although the shapes of the output responses plotted in Figs. 2–4 are reproduced by the model fits with appreciable accuracy, their peak amplitude is sometimes not perfectly matched by the model (see Fig. 2 *A*). These errors are, however, within the range of experimental variability of the system.

The similarity among the four sets of parameters in Table 1 suggests that the experiments of Figs. 2–4 can all be fit with a single set of parameters. When performing a simultaneous fit to data sets 1–4 (Table 1, Common column; see Fig. S5, Fig. S6, and Fig. S7), the agreement with the data is less precise than for fits to individual data sets. Nonetheless,

the predicted output currents are still qualitatively correct, despite the fact that the experiments were performed in OSNs from different species and with different stimuli. This indicates that indeed the model captures the relevant aspects of olfactory adaptation.

Another property of adaptation is the modification of the dynamical range of the input to which the system responds optimally. This modification causes a shift in the relation between the maximal amplitude of the current response and the input amplitude (the dose-response relation). The model here presented correctly reproduces this behavior (see Fig. S10).

DISCUSSION

The aim of this article is to formulate a basic model for adaptation in OSNs, able to capture all the kinetic features observed in the experiments and to provide a dynamical interpretation of the phenomenon. The main result is that both multipulse and step adaptation can be explained by the same assumption, namely that the dynamics of the feedback part of the pathway are much slower than those of the open-loop part. As mentioned in the Introduction, this scheme corresponds to an integral feedback with memory decay. That such a scheme can account for both types of adaptation is shown by best-fits of a kinetic model to experimental data.

One of the main predictions of our model is that the two forms of adaptation are in a dynamical trade-off: when the time constant of the feedback part becomes infinite and step adaptation is exact, then the recovery in multipulse adaptation vanishes; thus, the second pulse will have reduced amplitude for any interpulse interval (see Fig. S11, *A* and *B*). In terms of the model of Eqs. 1–7, a long feedback time constant means that the Ca-activated protein complexes responsible for the feedback are long-lived after the first pulse. Upon the arrival of a second pulse, their concentration is still high and the feedback-induced response attenuation is more rapid. When the feedback time constants are comparable to those of the open-loop part (see Fig. S11, *C* and *D*), then these complexes have time to dissociate before the arrival of the next pulse, and the response attenuation is diminished. For prolonged stimuli, the difference between the feedback and open-loop time constants determines the degree of adaptation.

In a model like that of Eqs. 1–7, a natural way to obtain slow dynamics for a state variable is to choose a time constant that is long (longer than the other time constants of the system), and feedback loops are natural candidates for slower kinetics, especially in the presence of output responses exhibiting only a transient excursion as in step adaptation. For our adaptation experiments, the identification of two slow variables appears to be confirmed by the agreement of fits performed independently on four data sets: all of them implicate CaBP- and CaCaM-mediated feedback as candidates. The high correlation among the four sets of parameters in Table 1 and the qualitatively correct fit obtained from simultaneous fitting of all four data sets emphasize that all of the experimental results we have presented can be accounted for by one model and that the trade-off mentioned earlier leaves only a limited parameter range compatible with both types of adaptation (the parameter space is explored in some details in the Supporting Material). Other well-known features of adaptation, such as the dose-response shift, are qualitatively reproduced by the model with best-fit parameters (see Fig. S10 and Table S2). In addition, the slow attenuation of the current response following a transient input in low extracellular Ca is replicated by the Eqs. 1–7 when the amount of Ca is set equal to zero (see Fig. S2).

Other models for olfactory transduction have been published in recent years (10,11,35). In Dougherty et al. (10) for instance, the authors focus on modeling multiple aspects of the kinetics, such as the plateau phase of the pulse response appearing on (some) high amplitude stimuli, and the onset of oscillations for step responses (see also the model in Reidl et al. (11)), from experiments using the suction-pipette technique (9,36). Neither of these features is present in the voltage-clamp experiments described here (the oscillations visible in the step adaptation of Fig. 2 are very small and irregular). In Dougherty et al. (10), capturing such complex phenomena requires a much more complicated model, with several nonlinear kinetic functional forms and several more parameters than the model developed here. This makes it more difficult to understand which basic mechanisms are responsible for adaptation. The model of Reidl et al. (11) instead represents an ionic channel with a three-conformation model: open, closed, and inhibited, the last corresponding to a nonconductive channel. In this model, the binding of Ca to the Ca-binding proteins present on the channel, initiates a refractory period in which the channel has lost sensitivity to cAMP and cannot reopen. This mechanism, in a way similar to what happens during the repolarization phase in models of neuronal action potentials, is described in detail in the Supporting Material (see also Fig. S13). The duration of the refractory period plays the same role as the long (feedback) time constant in a model like that of Eqs. 1–7.

As for adaptation in general, many mathematical models have been proposed in recent years (2,4,5,12–14). These are, however, exclusively concerned with step adaptation, and, as the exact integral feedback model shows, they may not manifest both forms of adaptation observed in olfactory transduction. From a kinetic point of view, the integral feedback model corresponds to a time constant that is infinite and induces an exact recovery to the prestimulus level (a perfect step adaptation), never observed in voltage-clamp measurements of olfactory transduction. That the inexact adaptation in our measurements is not an artifact is confirmed by the fact that the steady-state displacement scales

with the amplitude of the step input (see, for example, Fig. 1 of Menini et al. (15)). This property is not observed in perfect step adaptation, which is instead independent of input size—the displacement converges to zero for all amplitudes of the input step. Note that a dependence of the steady-state displacement on the amplitude of the constant input is captured by our model (see Fig. S12).

Despite these differences, a common principle in many adaptation models, namely that adaptation is the result of multiple timescales acting on a system (13,14), also guides our work. In the context of olfactory transduction, previous studies (21) have suggested that a slower kinetics is due to the action of CaMKII on AC, and that each form of adaptation is due to a different feedback (37). Our model suggests instead that a feedback on AC is not necessary and that, rather than a neat association of each form of adaptation to a particular feedback mechanism, there is a redundancy in the regulation, with each feedback contributing to both types of adaptation and only a marginal synergistic effect observable from their joint action. In our model this redundancy is highlighted by the observation that the only parameter that can be modified significantly without altering the quality of the fit is λ_3 (the dissociation rate of the CaCaM feedback). Provided that the time constant of the kinetics of the CaBP feedback is kept in the correct time window (i.e., slower than the time constant of Ca but fast enough to avoid perfect adaptation), λ_3 can be modified without drastically altering the closed loop behavior. Although a redundant role for the two feedback loops is a plausible hypothesis, its complete experimental validation is still unfeasible. In fact, if the CaCaM feedback loop can be blocked (as in our 8-Br-cAMP experiments), the blockage of the CaBP regulation requires the knowledge of all gating proteins naturally bound to the CNG channel—knowledge that is still out of reach.

SUPPORTING MATERIAL

Thirteen figures, two tables, and references (39–47) are available at http://www.biophysj.org/biophysj/supplemental/S0006-3495(12)00514-0.

This work was supported in part by a PRIN grant from the Ministero dell'Istruzione, dell'Università e della Ricerca.

REFERENCES

1. Torre, V., J. F. Ashmore, …, A. Menini. 1995. Transduction and adaptation in sensory receptor cells. *J. Neurosci.* 15:7757–7768.
2. Behar, M., N. Hao, …, T. C. Elston. 2007. Mathematical and computational analysis of adaptation via feedback inhibition in signal transduction pathways. *Biophys. J.* 93:806–821.
3. Shepherd, G. M. 1994. Neurobiology, 3rd ed. Oxford University Press, New York.
4. Alon, U., M. G. Surette, …, S. Leibler. 1999. Robustness in bacterial chemotaxis. *Nature.* 397:168–171.
5. Yi, T. M., Y. Huang, …, J. Doyle. 2000. Robust perfect adaptation in bacterial chemotaxis through integral feedback control. *Proc. Natl. Acad. Sci. USA.* 97:4649–4653.
6. Kurahashi, T., and T. Shibuya. 1990. Ca^{2+}-dependent adaptive properties in the solitary olfactory receptor cell of the newt. *Brain Res.* 515:261–268.
7. Kurahashi, T., and A. Menini. 1997. Mechanism of odorant adaptation in the olfactory receptor cell. *Nature.* 385:725–729.
8. Lagostena, L., and A. Menini. 2003. Whole-cell recordings and photolysis of caged compounds in olfactory sensory neurons isolated from the mouse. *Chem. Senses.* 28:705–716.
9. Reisert, J., and H. R. Matthews. 1999. Adaptation of the odor-induced response in frog olfactory receptor cells. *J. Physiol.* 519:801–813.
10. Dougherty, D. P., G. A. Wright, and A. C. Yew. 2005. Computational model of the cAMP-mediated sensory response and calcium-dependent adaptation in vertebrate olfactory receptor neurons. *Proc. Natl. Acad. Sci. USA.* 102:10415–10420.
11. Reidl, J., P. Borowski, …, M. Eiswirth. 2006. Model of calcium oscillations due to negative feedback in olfactory cilia. *Biophys. J.* 90:1147–1155.
12. Tyson, J. J., K. C. Chen, and B. Novak. 2003. Sniffers, buzzers, toggles and blinkers: dynamics of regulatory and signaling pathways in the cell. *Curr. Opin. Cell Biol.* 15:221–231.
13. Alon, U. 2006. An Introduction to Systems Biology: Design Principles of Biological Circuits. Chapman & Hall/CRC Mathematical & Computational Biology Series, 1st ed. Chapman and Hall/CRC, Boca Raton, FL.
14. Friedlander, T., and N. Brenner. 2009. Adaptive response by state-dependent inactivation. *Proc. Natl. Acad. Sci. USA.* 106:22558–22563.
15. Menini, A., C. Picco, and S. Firestein. 1995. Quantal-like current fluctuations induced by odorants in olfactory receptor cells. *Nature.* 373:435–437.
16. Schild, D., and D. Restrepo. 1998. Transduction mechanisms in vertebrate olfactory receptor cells. *Physiol. Rev.* 78:429–466.
17. Kleene, S. J. 2008. The electrochemical basis of odor transduction in vertebrate olfactory cilia. *Chem. Senses.* 33:839–859.
18. Takeuchi, H., and T. Kurahashi. 2002. Photolysis of caged cyclic AMP in the ciliary cytoplasm of the newt olfactory receptor cell. *J. Physiol.* 541:825–833.
19. Leinders-Zufall, T., C. A. Greer, …, F. Zufall. 1998. Imaging odor-induced calcium transients in single olfactory cilia: specificity of activation and role in transduction. *J. Neurosci.* 18:5630–5639.
20. Boccaccio, A., L. Lagostena, …, A. Menini. 2006. Fast adaptation in mouse olfactory sensory neurons does not require the activity of phosphodiesterase. *J. Gen. Physiol.* 128:171–184.
21. Leinders-Zufall, T., M. Ma, and F. Zufall. 1999. Impaired odor adaptation in olfactory receptor neurons after inhibition of Ca^{2+}/calmodulin kinase II. *J. Neurosci.* 19:RC19.
22. Kurahashi, T. 1989. Activation by odorants of cation-selective conductance in the olfactory receptor cell isolated from the newt. *J. Physiol.* 419:177–192.
23. Firestein, S., C. Picco, and A. Menini. 1993. The relation between stimulus and response in olfactory receptor cells of the tiger salamander. *J. Physiol.* 468:1–10.
24. Bradley, J., W. Bönigk, …, S. Frings. 2004. Calmodulin permanently associates with rat olfactory CNG channels under native conditions. *Nat. Neurosci.* 7:705–710.
25. Balasubramanian, S., J. W. Lynch, and P. H. Barry. 1996. Calcium-dependent modulation of the agonist affinity of the mammalian olfactory cyclic nucleotide-gated channel by calmodulin and a novel endogenous factor. *J. Membr. Biol.* 152:13–23.
26. Biskup, C., J. Kusch, …, K. Benndorf. 2007. Relating ligand binding to activation gating in CNGA2 channels. *Nature.* 446:440–443.

27. Nache, V., E. Schulz, …, K. Benndorf. 2005. Activation of olfactory-type cyclic nucleotide-gated channels is highly cooperative. *J. Physiol.* 569:91–102.

28. Trudeau, M. C., and W. N. Zagotta. 2003. Calcium/calmodulin modulation of olfactory and rod cyclic nucleotide-gated ion channels. *J. Biol. Chem.* 278:18705–18708.

29. Park, H. Y., S. A. Kim, …, L. Pollack. 2008. Conformational changes of calmodulin upon Ca^{2+} binding studied with a microfluidic mixer. *Proc. Natl. Acad. Sci. USA*. 105:542–547.

30. Boccaccio, A., and A. Menini. 2007. Temporal development of cyclic nucleotide-gated and Ca^{2+}-activated Cl− currents in isolated mouse olfactory sensory neurons. *J. Neurophysiol.* 98:153–160.

31. Suzuki, N., M. Takahata, and K. Sato. 2002. Oscillatory current responses of olfactory receptor neurons to odorants and computer simulation based on a cyclic AMP transduction model. *Chem. Senses.* 27:789–801.

32. Valsamis, J., J. Van Peborgh, and H. Brauman. 1986. Relative contribution of various expressions of cAMP excretion to other indices of parathyroid function, as tested by discriminant multivariate linear regression analysis. *Clin. Chem.* 32:1279–1284.

33. Butt, E., D. Pöhler, …, B. Bucher. 1995. Inhibition of cyclic GMP-dependent protein kinase-mediated effects by (Rp)-8-bromo-PET-cyclic GMPS. *Br. J. Pharmacol.* 116:3110–3116.

34. Gu, Y., P. Lucas, and J. P. Rospars. 2009. Computational model of the insect pheromone transduction cascade. *PLOS Comput. Biol.* 5:e1000321.

35. Halnes, G., E. Ulfhielm, …, J. P. Rospars. 2009. Modeling and sensitivity analysis of the reactions involving receptor, G-protein and effector in vertebrate olfactory receptor neurons. *J. Comput. Neurosci.* 27:471–491.

36. Reisert, J., and H. R. Matthews. 2001. Responses to prolonged odor stimulation in frog olfactory receptor cells. *J. Physiol.* 534:179–191.

37. Zufall, F., and T. Leinders-Zufall. 2000. The cellular and molecular basis of odor adaptation. *Chem. Senses.* 25:473–481.

38. Pifferi, S., A. Boccaccio, and A. Menini. 2006. Cyclic nucleotide-gated ion channels in sensory transduction. *FEBS Lett.* 580:2853–2859.

39. Borisy, F. F., G. V. Ronnett, …, S. H. Snyder. 1992. Calcium/calmodulin-activated phosphodiesterase expressed in olfactory receptor neurons. *J. Neurosci.* 12:915–923.

40. Chen, T. Y., and K. W. Yau. 1994. Direct modulation by Ca^{2+}-calmodulin of cyclic nucleotide-activated channel of rat olfactory receptor neurons. *Nature.* 368:545–548.

41. Wei, J., A. Z. Zhao, …, D. R. Storm. 1998. Phosphorylation and inhibition of olfactory adenylyl cyclase by CaM kinase II in neurons: a mechanism for attenuation of olfactory signals. *Neuron.* 21:495–504.

42. Matthews, H. R., and J. Reisert. 2003. Calcium, the two-faced messenger of olfactory transduction and adaptation. *Curr. Opin. Neurobiol.* 13:469–475.

43. Getchell, T. V. 1986. Functional properties of vertebrate olfactory receptor neurons. *Physiol. Rev.* 66:772–818.

44. Ottoson, D. 1955. Analysis of the electrical activity of the olfactory epithelium. *Acta Physiol. Scand. Suppl.* 35:1–83.

45. Getchell, T. V., and G. M. Shepherd. 1978. Adaptive properties of olfactory receptors analyzed with odor pulses of varying durations. *J. Physiol.* 282:541–560.

46. Pun, R. Y., and S. J. Kleene. 2003. Contribution of cyclic-nucleotide-gated channels to the resting conductance of olfactory receptor neurons. *Biophys. J.* 84:3425–3435.

47. Takeuchi, H., and T. Kurahashi. 2005. Mechanism of signal amplification in the olfactory sensory cilia. *J. Neurosci.* 25:11084–11091.